A Push–Pull Parallel Resonant Converter-Based Bidirectional IPT System

Lei Zhao, *Member, IEEE*, Duleepa J. Thrimawithana, *Senior Member, IEEE*, Udaya Kumara Madawala, *Fellow, IEEE*, and Aiguo Patrick Hu, *Senior Member, IEEE*

***Abstract*—Bidirectional inductive power transfer (BD-IPT) systems facilitate wireless grid integration of electric vehicles to offer vehicle-to-grid (V2G) services. This paper presents a novel push–pull parallel resonant converter-based BD-IPT system to provide a more efficient and cost-effective solution to wireless V2G technologies. The proposed system integrates the functionality of bulky passive elements into a double-D type magnetic coupler to achieve high power density. A phase-delay control technique is proposed to reduce the startup transients as well as to regulate bidirectional power flow between the primary and secondary sides of the push–pull converters. A zero-voltage switching zone is identified to maintain safe operation of the system. Both the operating principles and control philosophy of the converters are described, and a detailed mathematical analysis is presented. The effectiveness of the proposed system is verified by building a 3.3-kW prototype system. The experimental results show that the peak power transfer efficiency reaches 96.5%, and the efficiency remains high under a wide range of operating conditions.**

***Index Terms*—Inductive power transfer (IPT), push–pull parallel-resonant converter (PPRC), wireless power transfer.**

I. Introduction

ELECTRIC vehicles (EVs) are increasingly used as supplementary energy storage in distributed generation systems as well as service providers in smart grids [1], [2]. This concept is usually referred to as vehicle-to-grid (V2G) services [3]. A V2G system essentially requires a bidirectional power interface between the smart grid and the EV battery to provide services such as demand management, backup power, voltage-ampere (VA) injection, and harmonic compensation [1]–[3].

Traditional bidirectional ac–dc power converter topologies can be used to implement a plug-in interface between the grid and the EV as discussed in [1]–[3]. However, the preferred choice is now shifting toward the use of bidirectional inductive power transfer (BD-IPT) technology, to realize a "wireless" V2G system [4]–[7]. BD-IPT-based wireless V2G systems offer a safe, convenient, and efficient means to use an EV for providing grid services while being somewhat tolerant to misalignment between couplers [7]–[9].

A BD-IPT-based wireless V2G system consists of a grid-connected primary circuitry that produces a high-frequency ac voltage to drive the primary magnetic coupler through a compensation network. The primary circuitry typically composes a bidirectional grid-tied inverter that derives power from the grid and generates a regulated dc-link voltage. A full-bridge voltage-source inverter (VSI), which is supplied by this dc-link voltage, produces a phase-shift modulated ac voltage at a frequency, f_{sw} [7], [10]. To comply with SAE J2954 typically, f_{sw} is fixed at 85 kHz or maintained in the range of 81.38–90 kHz. The high-frequency ac voltage drives the primary coupler through a compensation network, which is tuned to f_{sw}. The pickup circuitry, which is connected to the EV battery, is somewhat similar to the primary circuitry, and includes a full-bridge VSI, a magnetic coupler, and a compensation network. Typically, the pickup VSI is operated at a fixed $\pm 90^{\circ}$ phase-delay with respect to the primary VSI to control the direction of power flow [8], [11]. The magnitude of power is controlled by varying the phase-shift modulation applied to the VSIs [12], [13].

The selection of compensation networks as well as the design of the magnetic couplers plays a vital role in the performance of the overall system. As such, over the last decade, many types of compensation networks suitable for BD-IPT applications, ranging from simple inductor–capacitor–inductor (*LCL*) networks to more complex hybrid and integrated tuning networks, have been developed [8], [11], [14]. Similarly, BD-IPT systems with polarized, nonpolarized, and multiphase magnetic couplers have been studied in search for low-cost solutions with improved misalignment tolerance [14]–[16]. However, the majority of this work reported to-date has been with regards to BD-IPT systems that employ VSIs.

A BD-IPT system that employs current-source inverters (CSIs) in both the primary and the pickup circuits is investigated in [17] and [18]. Full- and half-bridge-based CSIs are used to drive the primary and the pickup couplers that are parallel (*LC*) compensated [19]. The ability to efficiently control the magnitude and direction of power flow through the phase-delay between CSIs is illustrated mathematically as well as experimentally in [17] and [18]. Although the performance of these systems is somewhat comparable to a traditional VSI-based

Manuscript received March 16, 2019; revised June 3, 2019; accepted July 4, 2019. Date of publication July 22, 2019; date of current version December 13, 2019. Recommended for publication by Associate Editor M. Duffy. *(Corresponding author: Lei Zhao.)*

The authors are with Electrical, Computer, and Software Engineering, The University of Auckland, Auckland 1010, New Zealand (e-mail: lzha915@aucklanduni.ac.nz; d.thrimawithana@auckland.ac.nz; u.madawala@auckland.ac.nz; a.hu@auckland.ac.nz).

This paper has supplementary downloadable material available at http://ieeexplore.ieee.org, provided by the authors.

Color versions of one or more of the figures in this paper are available online at http://ieeexplore.ieee.org.

Digital Object Identifier 10.1109/TPEL.2019.2930283

BD-IPT system, the full or half-bridge CSIs require relatively large dc inductors [17]–[19].

Current sourced push–pull converters-based unidirectional IPT systems have been widely used in many commercial applications since early 1990s. For example, autonomous push–pull parallel-resonant converters (PPRCs) have been adopted to drive the primary couplers used in applications such as implantable devices, materials handling systems, artificial guided vehicles (AGVs), tunnel lighting, etc. [20]–[23]. However, unfortunately, these conventional PPRCs present a number of notable drawbacks in comparison to modern VSI-based systems, especially in EV charging applications [24]–[26]. The zero-voltage switching (ZVS) frequency of a conventional PPRC can change considerably with the output power as well as the misalignment between the couplers and can fall outside of the frequency range allowed by SAE J2954. In addition, a bulky dc inductor and a transformer are typically employed increasing the total cost of the system. As such, to-date, the PPRC technology has not been studied for practical wireless V2G systems.

This paper proposes a cost-effective and efficient PPRC-based BD-IPT system to address the issues identified above. The primary and the pickup PPRCs of this system are operated at a fixed frequency, $f_{\rm sw}$, and the relative phase-delay between the primary and pickup converters is used to minimize startup transients, ensure ZVS, and to regulate the power flow. A polarized DD-type magnetic coupler is employed, which also replaces the bulky dc inductor and the transformer. A detailed mathematical model of the proposed PPRC-based BD-IPT system, including the aspects that influence design, optimization, and control, is presented in this paper. The ZVS operating region of the system is analyzed using the model to show that the relative phase-delay between the two PPRCs is used to control power flow as well as to achieve ZVS under misaligned conditions. Moreover, this paper investigates how the voltage switch stresses can be distributed by using series-connected switches with parallel compensation capacitors to employ standard devices in PPRCs. Experimental results gathered from a 3.3-kW prototype are presented to validate accuracy of the mathematical analysis as well as to illustrate the ability of the PPRC-based BD-IPT system to maintain high efficiency within a designed operating region.

II. Proposed PPRC-Based IPT System

A. System Structure and Operating Principle

As shown in Fig. 1, the proposed system utilizes polarized DD-type magnetic couplers, which allow the integration of the dc-link inductor, current-splitting transformer, and the magnetic coupler into a single DD-type magnetic coupler [16], [25]. In a similar manner to conventional bidirectional IPT systems, the proposed system also employs identical circuitry and magnetics on the pickup side. The primary and pickup DD-type magnetic couplers are built from two coplanar D-shaped windings, $L_{pt,1}$ and $L_{pt,3}$, and $L_{st,2}$ and $L_{st,4}$, respectively. The mutual inductances M_{12} and M_{34} model the main coupling; M_{23} and M_{14} model the cross coupling; and M_{13} and M_{24} model the intercoupling as shown in Fig. 1. The primary magnetic coupler is parallel compensated using C_{pt}, C_{pa}, C_{pb}, C_{pc}, and C_{pd}.

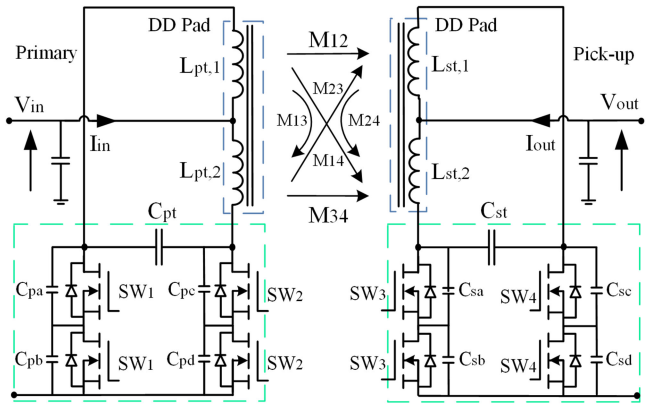

Fig. 1. Proposed PPRC-based BD-IPT system.

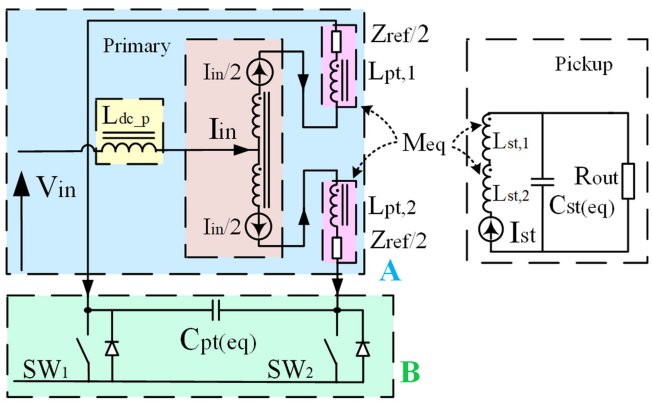

Fig. 2. Equivalent circuit of the PPRC-based BD-IPT system.

Similarly, the pickup magnetic coupler is parallel compensated using C_{st}, C_{sa}, C_{sb}, C_{sc}, and C_{sd}. Fig. 2 shows an equivalent circuit of the primary PPRC, which consist of part "A," a multifunctional DD coupler; and part "B," a push–pull converter and a parallel compensation capacitor. The multifunctional primary DD-type magnetic coupler is center tapped and connected to a dc voltage source, $V_{\rm in}$. The two ends of the coplanar D-shaped windings are driven 180° apart by switches $\rm SW_1$ and $\rm SW_2$. $I_{\rm in}$ can be assumed to be equally divided between the two coplanar windings. Since the current in each coplanar winding is 180° apart the coupler operates in the DD mode generating a single-sided flux pattern between the north and south poles created by the coplanar D-shaped windings. The resulting ac magnetic field transfers power wirelessly to the pickup, which can be modeled using a reflected impedance, $Z_{\rm ref}$. To analyse the primary PPRC, the pickup PPRC can be simply modeled as a parallel resonant circuit with an equivalent load resistance, $R_{\rm out}$, that is independent of $f_{\rm ws}$.

B. DD-Type Magnetic Coupler Parameters

As shown in Fig. 3, the self- and mutual inductances of the DD-type magnetic couplers were measured and recorded within the range of 0–160 mm horizontal (Y-axis) and 100–140 mm vertical (Z-axis) displacements using an Agilent LCR meter.

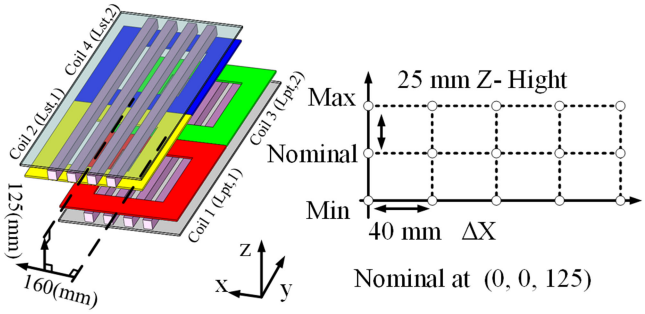

Fig. 3. DD-type couplers used in the PPRC-based BD-IPT system.

TABLE I
MUTUAL INDUCTANCE VALUES OF THE DD COUPLERS

Z (mm)	M (μH)	X (mm)				
		0	40	80	120	160
100	$M_{12} \approx M_{34}$	28.2	27.2	24.8	21.1	16.6
	$M_{13} \approx M_{24}$	15.6	15.2	15.0	14.3	13.4
	$M_{23} \approx M_{14}$	11.8	11.5	9.9	9.2	7.7
120	$M_{12} \approx M_{34}$	23.6	22.7	20.5	17.7	13.9
	$M_{13} \approx M_{24}$	14.5	14.3	13.7	13.5	12.9
	$M_{23} \approx M_{14}$	10.1	9.9	9.2	8.0	6.5
140	$M_{12} \approx M_{34}$	18.6	18.2	17.0	14.9	12.3
	$M_{13} \approx M_{24}$	13.5	13.3	13.1	12.9	12.4
	$M_{23} \approx M_{14}$	8.2	8.1	7.7	6.8	5.9

The position at which each magnetic coupler is fully compensated is chosen as the position where the pickup magnetic coupler is placed 120 mm directly above the primary magnetic coupler. The strongest coupling between the magnetic couplers is when the pickup magnetic coupler is located at (0, 0, 100), where both M_{12} and M_{34} are approximately 28.2 μH. The lowest coupling between the couplers is observed when increasing vertical and horizontal displacements to (160, 0, 140), where both M_{12} and M_{34} drop to 12.3 μH. In contrast, the changes in intercoupling and cross coupling with displacement are relatively small, varying from 15.6 to 12.4 μH, and from 11.8 to 5.9 μH, respectively. The self-inductance of the magnetic couplers also varies from 84.1 μH at (0, 0, 100) to 79.6 μH at (160, 0, 140). Mutual inductance (M) values between the windings of the couplers are summarized in Table I.

Using the parameters listed in Table I, an equivalent mutual inductance matrix that models the coupled windings depicted in Fig. 3 can be derived as given as

$$M_{DD} = \begin{bmatrix} L_{pt,1} + L_{pt,2} + 2M_{13} & M_{\text{eq}} \\ M_{\text{eq}} & L_{st,1} + L_{st,2} + 2M_{24} \end{bmatrix} \quad (1)$$

where the main-, inter-, as well as cross-coupling between the coupled windings can be expressed as

$$M_{\text{eq}} = M_{12} + M_{34} + M_{23} + M_{14}. \quad (2)$$

The equivalent self-inductances of the primary and pickup couplers are therefore $L_{pt,1} + L_{pt,2} + 2M_{13}$ and $L_{st,1} + L_{st,2} + 2M_{24}$, respectively. Since the two windings of the primary as well as the pickup DD magnetic couplers are loosely coupled to each other, the leakage-flux paths present effective

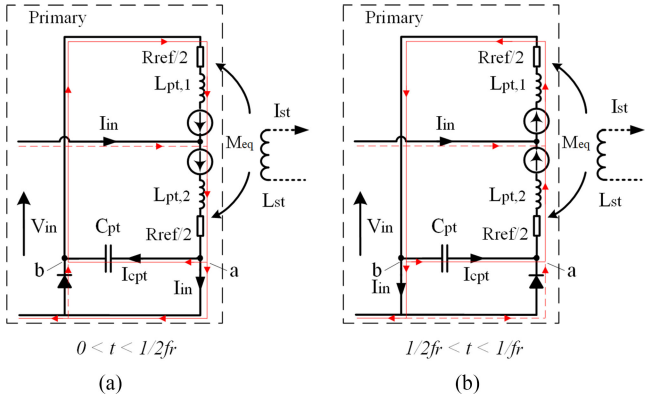

Fig. 4. Equivalent circuit models during each half-cycle.

inductances, $L_{\text{dc\_}p}$ and $L_{\text{dc\_}s}$, to the common mode dc currents, I_{in} and I_{out}, respectively. $L_{\text{dc\_}p}$ and $L_{\text{dc\_}s}$ are given by

$$L_{\text{dc\_}p} = \frac{\sqrt{L_{pt,1} \cdot L_{pt,2}} - M_{13}}{2} \quad (3)$$

$$L_{\text{dc\_}s} = \frac{\sqrt{L_{st,1} \cdot L_{st,2}} - M_{24}}{2}. \quad (4)$$

C. Converter and Tuning

To ensure SW_1 and SW_2 of the primary PPRC shown in Fig. 2 achieve ZVS, $C_{pt(\text{eq})}$ is selected such that the resonant frequency of the primary is higher than the switching frequency as given by

$$C_{pt(\text{eq})} \le \frac{\psi}{(2\pi f_r)^2 \left[(L_{pt,1} + L_{pt,2} + 2M_{13})\,\psi - M_{\text{eq}}^2\right]} \quad (5)$$

where f_r is the damped resonant frequency given by (16) and $\psi = (L_{st,1} + L_{st,2} + 2M_{24})$. $C_{pt(\text{eq})}$ is formed by C_{pt} together with the voltage balancing capacitors $C_{pa} = C_{pb} = C_{pc} = C_{pd} = C_p$ that in parallel across the switches as shown in Fig. 1. Therefore, it is given by

$$C_{pt(\text{eq})} = C_{pt} + \frac{1}{2}\left(\frac{C_{pa} \cdot C_{pb}}{C_{pa}+C_{pb}} + \frac{C_{pc} \cdot C_{pd}}{C_{pc} + C_{pd}}\right) = C_{pt} + \frac{C_p}{2}. \quad (6)$$

Similarly, C_{st}, C_{sa}, C_{sb}, C_{sc}, and C_{sd} can be derived to ensure SW_3 and SW_4 operated under ZVS conditions. It should be noted that if the resonant frequency is lower than switching frequency, the capacitors will have charge when the switches turn ON. Thus, the switches would dissipate the energy stored in the resonant capacitors and the switches will not operate under ZVS condition.

III. MATHEMATICAL MODELING AND ANALYSIS

In order to gain an insight into the operation of the proposed system, a closed-form mathematical model is derived following the process discussed in [22]–[24]. The switches of the proposed PPRC-based BD-IPT system are operated at a frequency, f_{sw}, which is lower than the damped resonant frequency, f_r. Due to the symmetric nature of each half-cycle, as shown in Fig. 4, only

the first half of a switching time period is considered assuming that at 0 s, SW_1 is turned OFF and SW_2 is tuned ON. Applying KCL to the equivalent circuit model at node "a" shown by Fig. 4 results in

$$i_{Cpt} + i_{Lpt} = \frac{I_{\rm DC}}{2}. \tag{7}$$

The voltage, v_{cpt}, and current, i_{cpt}, of $C_{pt(\rm eq)}$ are related by

$$C_{pt(\rm eq)} \frac{dv_{Cpt}}{dt} = i_{Cpt}. \tag{8}$$

The voltage across L_{pt} is given by

$$v_{Lpt} = L_{pt} \frac{di_{Lpt}}{dt}. \tag{9}$$

As discussed previously, the equivalent self-inductances of the primary are

$$L_{pt} = L_{pt,1} + L_{pt,2} + 2M_{13}. \tag{10}$$

The induced voltage across each winding in the primary DD coupler due the pickup is given by

$$v_{\rm ref} = i_{Lpt} \cdot Z_{\rm ref} \tag{11}$$

where $Z_{\rm ref}$ models the impedance reflected on to the primary by pickup. The real component of $Z_{\rm ref}$ is given by

$$\mathrm{Re}\{Z_{\rm ref}\} = \frac{(\omega_r M_{\rm eq})^2 \cdot R_{\rm out} \cdot \sin(\theta)}{R_{\rm out}(1-\omega_r^2 L_{st} C_{st})^2 - (\omega_r L_{pt})^2} \tag{12}$$

where $M_{\rm eq}$ is given by (2), θ is the phase-delay applied to the pickup converter with respect to the primary converter, and $\omega_r = 2\pi f_r$. Therefore, by manipulating (7)–(12)

$$\frac{d^2 v_{Cpt}}{dt^2} + \frac{Z_{\rm ref}}{L_{pt}} \cdot \frac{dv_{Cpt}}{dt} + \frac{v_{Cpt}}{L_{pt} \cdot C_{pt(\rm eq)}} = \frac{i_{Cpt} \cdot Z_{\rm ref}}{L_{pt} \cdot C_{pt(\rm eq)}}. \tag{13}$$

The solution to (13) is in the form

$$v_{Cpt} = \sigma \cdot e^{\left(-\alpha + \sqrt{\alpha^2 - \omega_r^2}\right)t} + \kappa \cdot e^{\left(-\alpha - \sqrt{\alpha^2 - \omega_r^2}\right)t} \tag{14}$$

where σ and κ are constants defined by circuit conditions, while α and ω_r are given by

$$\alpha = \frac{L_{pt} R_{\rm out}\left(1-\omega_r^2 L_{st} C_{st}\right)^2 - (\omega_r L_{pt})^2}{2 \cdot (\omega_r M_{\rm eq})^2 \cdot R_{\rm out}} \tag{15}$$

$$\omega_r = \frac{1}{\sqrt{L_{pt} \cdot C_{pt(\rm eq)} \cdot \left(1 - \frac{M_{\rm eq}^2}{L_{pt}^2} \cdot \sin^2\theta + \frac{M_{\rm eq}}{L_{pt}} \cdot \cos\theta\right)}}. \tag{16}$$

If $Z_{\rm ref} > \sqrt{L_{pt}/(4 \cdot C_{pt(\rm eq)})}$, the resonant circuit is underdamped and oscillatory, and facilities the converter operation with ZVS. Under these conditions, (14) can be expressed as

$$v_{Cpt} = e^{-\alpha t} \begin{bmatrix} \sigma \cdot \cos\left(\sqrt{(\omega_r^2 - \alpha^2)} \cdot t\right) \\ +\kappa \cdot \sin\left(\sqrt{(\omega_r^2 - \alpha^2)} \cdot t\right) \end{bmatrix}. \tag{17}$$

If the initial voltage across C_{pt} is assumed to be zero, σ becomes zero, simplifying (17) to

$$v_{Cpt} = \kappa \cdot e^{-\alpha t} \sin\left(\sqrt{(\omega_r^2 - \alpha^2)}\, \frac{f_r}{f_{\rm sw}}\, t\right) \tag{18}$$

when $0 < t < 1/2f_r$.

κ can be evaluated by equating the steady-state volt–second product across $L_{\rm DC}$ to zero over a single switching period and is given by

$$\kappa = \pi V_{\rm in} \left(\frac{f_r}{f_{\rm sw}}\right) \left[\frac{2\left(\omega_r^2 + \alpha^2\right)}{\omega_z^2 \left(e^{\frac{-\alpha}{2f_r}} + 1\right)}\right]. \tag{19}$$

Substituting (19) into (18)

$$v_{Cpt} = \pi V_{\rm in} \left(\frac{f_r}{f_{\rm sw}}\right) \left[\frac{2\left(\omega_r^2 + \alpha^2\right)}{\omega_z^2 \left(e^{\frac{-\alpha}{2f_r}} + 1\right)}\right] \cdot e^{-\alpha t} \sin\left(\sqrt{(\omega_r^2 - \alpha^2)}\, \frac{f_r}{f_{\rm sw}} \cdot t\right). \tag{20}$$

A conventional push–pull converter is typically operated across a variable switching frequency band to facilitate ZVS. However, the switching frequency of the proposed PPRC-based BD-IPT system is held constant and θ is used to facilitate ZVS. The switches of the primary and pickup converters are operated at $f_{\rm sw}$, which is higher than f_r, with a duty cycle, D, of 0.5. Therefore, this may result in time period, T_{DB}, where both switches conduct, where T_{DB} is given by

$$T_{DB} = \frac{1}{2}\left(\frac{1}{f_{\rm sw}} - \frac{1}{f_r}\right). \tag{21}$$

During T_{DB}, one switch is turned ON and the body diode of the other switch conducts, shorting the two ends of the primary DD coupler to ground. This clamps voltage of the capacitor C_{pt} to zero, facilitating ZVS turn ON during the next half-period. $L_{\rm dc\_p}$ limits the rate of rise of current during T_{DB} and can be considered constant since T_{DB} is negligibly small. Therefore, using (7)–(13) and (20), the resonant current flowing through the primary coupler is derived as given by

$$i_{Lpt} = \frac{2\pi V_{\rm in} f_r}{L_{pt}\omega_r^2 \left(e^{\frac{-\alpha}{2f_r}} + 1\right) f_{\rm sw}} \times \left[\omega_r e^{-\alpha t}\cos(\zeta) + \alpha e^{-\alpha t}\sin(\zeta)\right] + \lambda \tag{22}$$

where ζ is derived as given by

$$\zeta = \sqrt{(\omega_r^2 - \alpha^2)}\, \frac{f_r}{f_{\rm sw}} \cdot t. \tag{23}$$

The resonant current flowing through L_{pt} at the end of each half-cycle should be equal in magnitude but opposite in direction as given by

$$i_{Lpt(\ t=0)} = -i_{Lpt\left(t=\frac{1}{2f_r}\right)}. \tag{24}$$

Apply (24) in (22), λ is derived as given by

$$\lambda = \left(\frac{f_r}{f_{\rm sw}}\right) \left[\frac{\pi V_{\rm in}\left(1 - e^{\frac{-\alpha}{2f_r}}\right)}{L_{pt}\omega_r \left(e^{\frac{-\alpha}{2f_r}} + 1\right)}\right]. \tag{25}$$

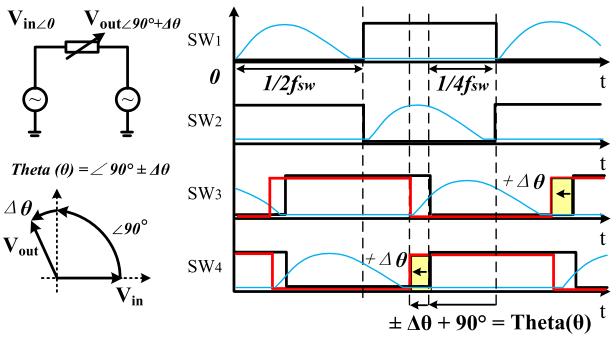

Fig. 5. Switching signals.

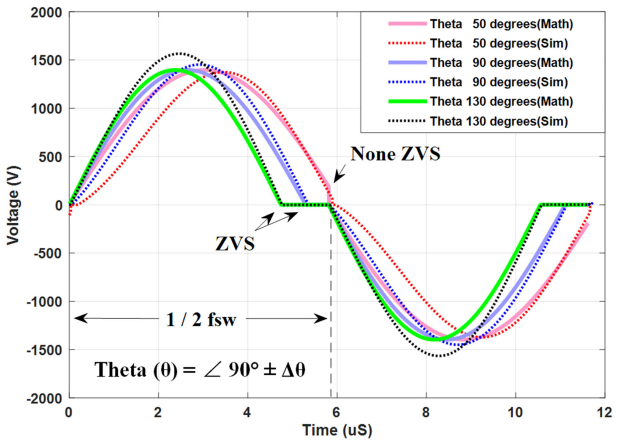

Fig. 6. Voltage across primary C_{pt} at position (0, 0, 100).

Substituting (23) and (25) into (22), the resonant current flowing through L_{pt} can be derived as

$$i_{Lpt} = \frac{2\pi V_{\text{in}} f_r}{L_{pt}\omega_r^2\left(e^{\frac{-\alpha}{2f_r}}+1\right)f_{\text{sw}}}\left[\omega_r e^{-\alpha t}\cos(\zeta) + \alpha e^{-\alpha t}\sin(\zeta)\right] + \left(\frac{f_r}{f_{\text{sw}}}\right)\left[\frac{\pi V_{\text{in}}\left(1-e^{\frac{-\alpha}{2f_r}}\right)}{L_{pt}\omega_r\left(e^{\frac{-\alpha}{2f_r}}+1\right)}\right]. \quad (26)$$

Since the dc inductor is integrated with the DD coupler, currents through each winding of the coupler should also conduct the dc current and can simply be obtained by

$$i_{Lpt,1} = i_{Lpt,2} = i_{Lpt} \pm \frac{i_{\text{DC}}}{2}. \quad (27)$$

The power delivered to the load could be calculated from (26) as given by

$$P_{\text{out}} = 2\cdot\int_0^{\frac{1}{2f_r}} (i_{Lpt,1}-i_{Lpt,2})^2\cdot\left(2\cdot\frac{Z_{\text{ref}}}{2}\right)dt = 8\cdot\Gamma\int_0^{\frac{1}{2f_r}}\left\{\left[e^{-\alpha t}\cos\left(\sqrt{(\omega_r^2-\alpha^2)}\,\frac{f_r}{f_{\text{sw}}}\cdot t\right)+\frac{\alpha}{\omega_r}e^{-\alpha t}\cdot\sin\left(\sqrt{(\omega_r^2-\alpha^2)}\,\frac{f_r}{f_{\text{sw}}}\cdot t\right)\right]+\left(1-e^{\frac{-\alpha}{2f_r}}\right)\right\}^2\cdot dt \quad (28)$$

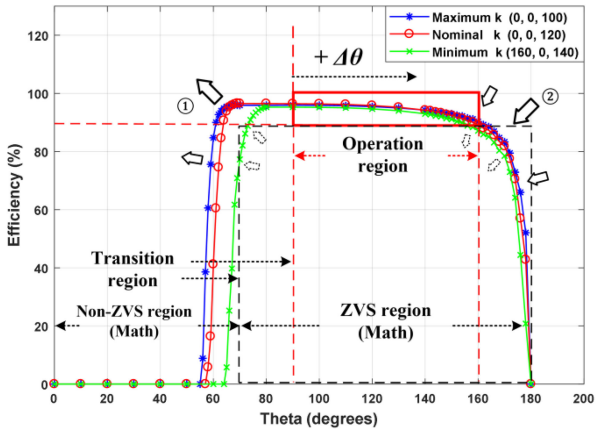

①. Efficiency increase as the coupling (M) between DD pads increase
②. Efficiency reduces as proportion of the conduction losses increase

Fig. 7. Efficiency against phase-delay θ.

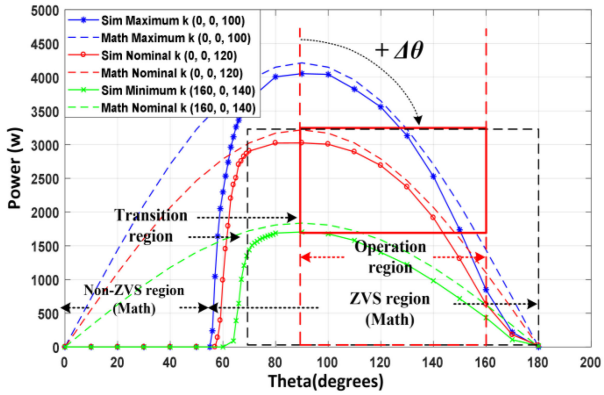

Fig. 8. Power against phase-delay θ.

where

$$\Gamma = \frac{\pi V_{\text{in}} f_r}{L_{pt}\omega_r\left(e^{\frac{-\alpha}{2f_r}}+1\right)f_{\text{sw}}}\cdot\frac{(\omega_r M_{\text{eq}})^2\cdot R_{\text{out}}\cdot\sin(\theta)}{R_{\text{out}}(1-\omega_r^2 L_{st}C_{st})^2+(\omega_r L_{pt})^2}.$$

IV. Power Flow Control

In a typical BD-IPT system, the phase-delay between the primary and pickup converters, θ, is usually used as a variable to control the direction of power flow [6], [7], [11], [12]. For example, as presented in [12], the voltage generated by the pickup converter is at $\pm 90°$ with respect to the voltage generated by the primary converter, resulting in power being transferred in forward or reverse direction across the air gap. The amplitude of the voltages generated by the primary and pickup converters is usually used to control the magnitude of power flow. In contrast, the magnitude and direction of power flow of the proposed PPRC-based BD-IPT system are controlled using θ, as derived in (28). The maximum power is transferred when θ is $\pm 90°$. As an example, Fig. 5 shows the switching waveforms when the

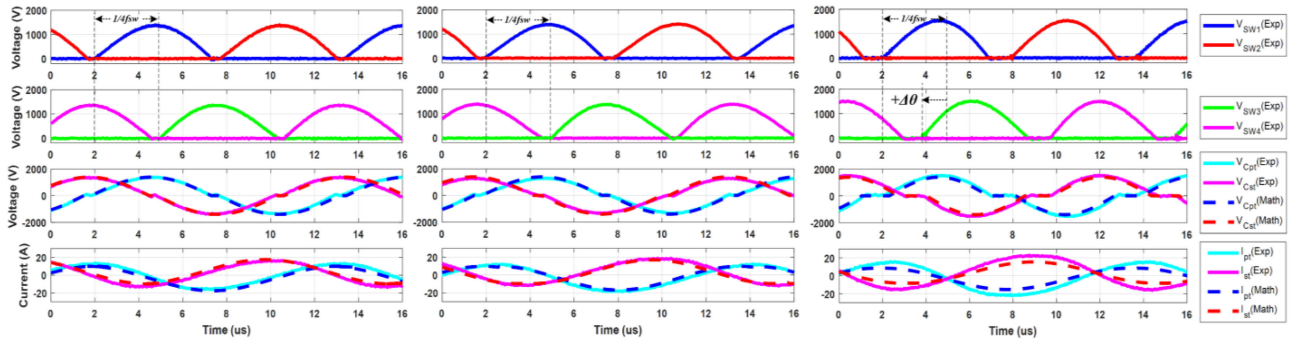

(a) (b) (c)

Fig. 9. Waveforms of the proposed prototype. (a) At position (160, 0, 140). (b) At position (0, 0, 120). (c) At position (0, 0, 100).

system is transferring maximum power to the pickup (i.e., $\theta =$ –90°).

To demonstrate the operation of the switches under ZVS conditions, the voltage across C_{pt} is depicted in Fig. 6 as a function of θ. In this example, the location of the pickup coupler was chosen as (0,0,100). To verify the accuracy of the mathematical model, the waveforms derived using (6)–(21) are compared against the simulated results generated from MATLAB PLECS, in the same figure. When the angle θ is set at 50°, the voltage waveform across C_{pt} is distorted and results in loss of ZVS. This indicates that some of the energy stored in $C_{pt(\mathrm{eq})}$ will be dissipated in the switches, drastically lowering the system efficiency. However, if the phase-delay, θ, is set to 90°, or 130°, $C_{pt(\mathrm{eq})}$ fully discharges before the turn-ON switching instant, thus, facilitating ZVS. Results also validate the accuracy of the mathematical model.

Fig. 7 shows the simulated dc/dc efficiency when pickup coupler is at (0, 0, 100), (0, 0, 125), and (160, 0, 140) as a function of θ. The theoretically calculated ZVS operating region is also shown in Fig. 7. It is evident from Fig. 7 that the converter exhibits ZVS when θ is between 70° and 180°.

According to (28), the power throughput can be changed by either increasing or decreasing θ. If θ is decreased, as can be seen in Fig. 7, the converters can operate in the transition region which lies in between the non-ZVS region and the recommended operating region. The boundary of the transition region is a function of coupling where an increase in coupling causes the transition region to expand, as indicated by the arrows labeled (1) in Fig. 7. The theoretical peak efficiency is observed when θ is decreased below 90°, as the switching frequency coincides with the damped resonant frequency. As evident from Fig. 7, the peak efficiency achievable will also increase as the coupling between the DD couplers increases. However, in this critical area, converter tends to lose ZVS if operating conditions change. Therefore, it is not recommended to operate the system in the transition region but rather to leave a safety margin for the controller.

As evident from Fig. 8, angle θ is increased beyond 90° to control the power transfer at position (0, 0, 100); the real power decreases according to (28) but the magnitude of resonant current remains nearly constant. Consequently, the conduction losses increase significantly lowering efficiency as indicated by the arrows labelled (2) in Fig. 7. However, according to the mathematical model, the converter maintains ZVS operation even when the angle θ is close to 180° and thus is the preferred region to operate when controlling the power transfer. In addition, θ can be decreased progressively from 180° toward 90° during startup to reduce transient oscillations and to avoid hard switching.

TABLE II
PARAMETERS OF THE PROPOSED BD-IPT SYSTEM

Parameter	Value	ESR
$L_{pt,1}$, $L_{pt,2}$	82.71 μH	130 mΩ
$L_{st,1}$, $L_{st,2}$	81.85 μH	122 mΩ
C_{pt}, C_{st}	17.8 nF	35.3 mΩ
C_{pa}, C_{pb}, C_{pc}, C_{pd}	1.0 nF	12.0 mΩ
C_{sa}, C_{sb}, C_{sa}, C_{sb}	1.0 nF	12.6 mΩ
V_{in} &V_{out}	400V	
f_s	86.0 kHz	
k (at nominal position)	0.27	

V. EXPERIMENTAL RESULTS

To validate both the operation and the proposed control scheme of a PPRC-based BD-IPT system, a 3.3-kW prototype has been designed, built, and tested. This proof-of-concept prototype system employed the pair of DD couplers that were introduced in Section II. The push–pull converters were built using C3M0065090D SiC MOSFET switches and the other key circuit parameters are listed in Table II.

Both the primary and the pickup were driven using open-loop controllers with a preprogrammed θ to regulate the output power to 3.3 kW as the position of the pickup coupler was changed in X and Z directions with respect to the primary coupler. Of the three pickup coupler operating positions investigated, the first position at (160, 0, 140) was considered as the worst coupling position, and the second position at (120, 0, 0) was considered as the nominal operating position while the (100, 0, 0) was considered as the best coupling position.

The resonant voltage and current waveforms of the proposed system operating at (160, 0, 140) are shown in Fig. 9(a).

The mathematical and experimental results align well, verifying the accuracy of the mathematical model. The compensation networks are tuned as per (4), where the selected C_{pt} leads to a short T_{DB} as evident from the V_{Cpt} and V_{Cst} waveforms. Since the pickup coupler is misaligned, the coupling is lower than the nominal value, and as a result θ is set at 90° to transfer 1.66 kW to the pickup side. The current in the couplers is also depicted in Fig. 9(a).

Fig. 9(b) depicts the resonant current and voltage waveforms at (0, 0, 120). As can be seen from the figure, θ is set at 90° to transfer 3.2 kW to the pickup side. When the pickup coupler is moved from (160, 0, 140) to (0, 0, 120), both self- and mutual inductances increase, which leads to an elongated V_{Cpt} and V_{Cst} waveforms. However, the converter operates in the ZVS region as discussed in Section IV. The prototype exhibits an efficiency of 96.5% at (0,0,120) and the losses mainly consist of conduction losses in the couplers and the switches. The switching loss is negligible due to ZVS.

As the pickup coupler moves to (0, 0, 100), the higher mutual inductance leads to an increase in power transfer. As discussed in Section IV, θ is controlled to lower power throughput to 3.3 kW. As evident from in Fig. 9(c), θ between the converters has been set to 127° in order to limit the power flow while ensuring ZVS. This leads to a longer T_{DB} as predicted using the mathematical model presented in the previous sections. As a result, the efficiency drops to 95.5%.

The efficiency of the PPRC-based BD-IPT prototype is shown Fig. 10(a). As evident from the figure, the efficiency of the PPRC-based BD-IPT system peaks at (0, 0, 120) while remaining high for all operating conditions considered. In comparison, the efficiency of an *LCL* BD-IPT system using identical couplers and switches is shown in Fig. 10(b). As evident from Fig. 10, the PPRC-based BD-IPT system offers approximately a 0.5–1.5% improvement in efficiency. This can be attributed to ZVS operation offered by the PPRC-based BD-IPT system under all operating conditions. It should be noted that both systems exhibit similar power profiles as coupling changes. The losses associated with the driver circuitry and the controllers are excluded as they are negligible.

The efficiency and power output of the proposed PPRC-based BD-IPT system are shown in Fig. 11, as a function of θ at (0, 0, 120). As expected from the simulation results in Fig. 8, the power output is zero when theta is set to 180°, which verifies the power flow control schemes discussed in Section IV. The power loss increases linearly, with increasing θ due to increasing conduction losses. The efficiency of the PPRC-based BD-IPT system decreases drastically when theta is over 160°, as conduction losses become significant. However, the push–pull converters always operate with ZVS.

Two C3M0065090D SiC switches were connected in series to construct the high-voltage switches in the PPRC using readily available devices. In practice, delays introduced by the driver circuitry as well as device tolerances cause voltage imbalances between series-connected switches. This can be overcome by using voltage balancing capacitors as shown in Fig. 1. As an example, the voltages across the two C3M0065090D switches

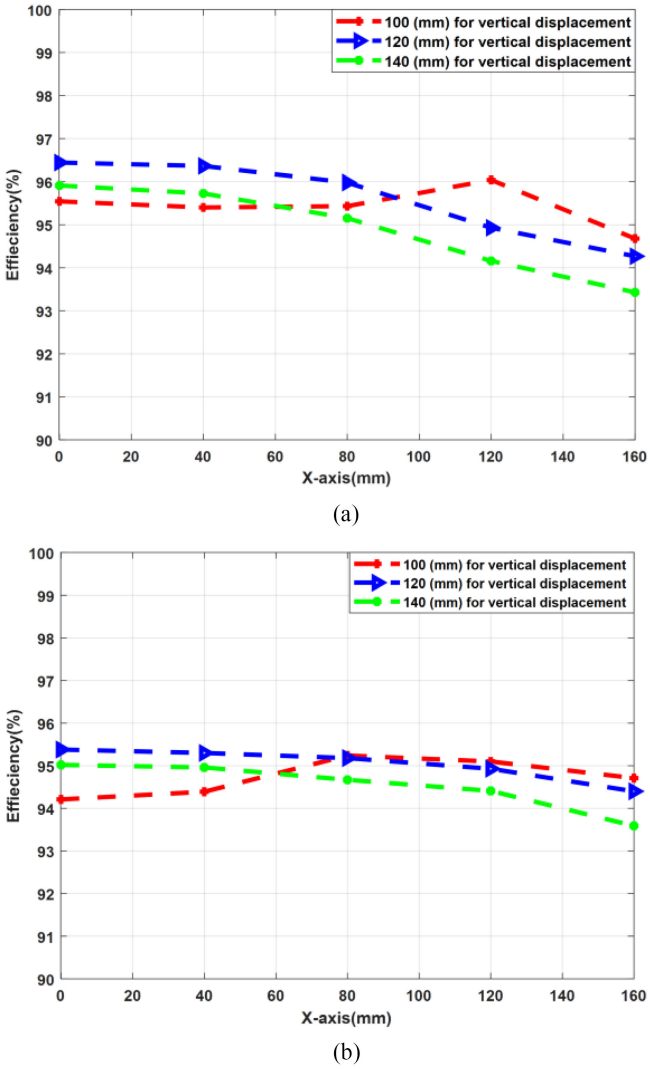

Fig. 10. Efficiency of BD-IPT systems. (a) PPRC-based BD-IPT system. (b) *LCL*-based BD-IPT system.

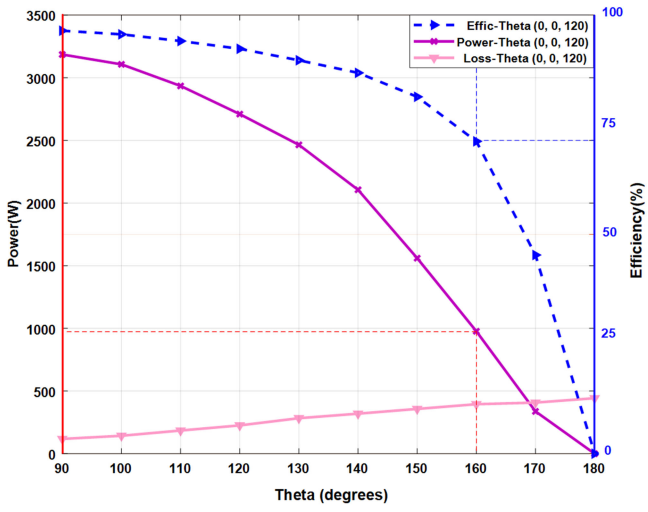

Fig. 11. Power and efficiency against θ at (0, 0, 120).

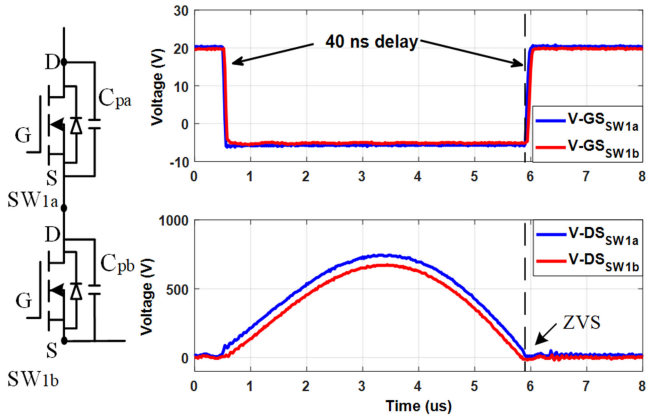

Fig. 12. Voltages across switches and driving signals.

that make up SW_1 are shown in Fig. 12. The voltage balancing capacitors, C_{pa} and C_{pb}, are helping to limit the voltage across each switch to approximately 0.5 πV_{in}. Since all switches are operated under ZVS condition, as evident from Fig. 12, slight delays or variations in device parameters do not make a significant change in voltage stress experienced by each switch.

VI. Conclusion

A PPRC-based BD-IPT system that employs DD magnetic couplers has been presented as a low cost and efficient wireless grid interface for V2G applications. The DD coupler integrates the functionality of the dc inductor and the current-splitting transformer used in a traditional PPRC, thereby reducing the number of components required. The phase-delay between the primary and the pickup PPRC has been used to control the power throughput while ensuring ZVS operation of the converters within the designed operating region. A mathematical model has been established to gain an insight into the performance of the system, and to define the ZVS operating region. Both theoretical and experimental results obtained from a 3.3-kW prototype, built with cascaded SiC switches, demonstrated that the proposed PPRC-based BD-IPT system can achieve an end-to-end power efficiency of 96.5%.

References

[1] K. Clement-Nyns, E. Haesen, and J. Driesen, "The impact of charging plug-in hybrid electric vehicles on a residential distribution grid," *IEEE Trans. Power Syst.*, vol. 25, no. 1, pp. 371–380, Feb. 2010.

[2] J. A. P. Lopes, F. J. Soares, and P. M. R. Almeida, "Integration of electric vehicles in the electric power system," *Proc. IEEE*, vol. 99, no. 1, pp. 168–183, Jan. 2011.

[3] C. Liu, K. Chau, D. Wu, and S. Gao, "Opportunities and challenges of vehicle-to-home, vehicle-to-vehicle, and vehicle-to-grid technologies," *Proc. IEEE*, vol. 101, no. 11, pp. 2409–2427, Nov. 2013.

[4] U. K. Madawala and D. J. Thrimawithana, "A bidirectional inductive power interface for electric vehicles in V2G systems," *IEEE Trans. Ind. Electron.*, vol. 58, no. 10, pp. 4789–4796, Oct. 2011.

[5] R. M. Miskiewicz, A. J. Moradewicz, and M. P. Kazmierkowski, "Contactless battery charger with bi-directional energy transfer for plug-in vehicles with vehicle-to-grid capability," in *Proc. IEEE Int. Symp. Ind. Electron.*, 2011, pp. 1969–1973.

[6] A. A. Mohamed, A. Berzoy, and O. A. Mohammed, "Experimental validation of comprehensive steady-state analytical model of bidirectional WPT system in EVs applications," *IEEE Trans. Veh. Technol.*, vol. 66, no. 7, pp. 5584–5594, Jul. 2017.

[7] X. Zhang *et al.*, "A control strategy for efficiency optimization and wide ZVS operation range in bidirectional inductive power transfer system," *IEEE Trans. Ind. Electron.*, vol. 66, no. 8, pp. 5958–5969, Aug. 2019.

[8] L. Zhao, D. J. Thrimawithana, and U. K. Madawala, "Hybrid bidirectional wireless EV charging system tolerant to pad misalignment," *IEEE Trans. Ind. Electron.*, vol. 64, no. 9, pp. 7079–7086, Sep. 2017.

[9] D. J. Thrimawithana and U. K. Madawala, "A contactless bi-directional power interface for plug-in hybrid vehicles," in *Proc. IEEE Vehicle Power Propulsion Conf.*, 2009, pp. 396–401.

[10] L. Zhao, D. J. Thrimawithana, U. K. Madawala, and C. A. Baguley, "Performance optimization of LC bi-directional inductive power transfer system," in *Proc. IEEE 13th Brazilian Power Electron. Conf. 1st Southern Power Electron. Conf.*, 2015, pp. 1–6.

[11] L. Zhao, D. J. Thrimawithana, and U. K. Madawala, "A comparison of LCL and LC bi-directional inductive power transfer systems," in *Proc. Int. Power Electron. Appl. Conf. Expo.*, 2014, pp. 766–771.

[12] D. J. Thrimawithana and U. K. Madawala, "A generalized steady-state model for bidirectional IPT systems," *IEEE Trans. Power Electron.*, vol. 28, no. 10, pp. 4681–4689, Oct. 2013.

[13] Y. Tang, Y. Chen, U. K. Madawala, D. J. Thrimawithana, and H. Ma, "A new controller for bidirectional wireless power transfer systems," *IEEE Trans. Power Electron.*, vol. 33, no. 10, pp. 9076–9087, Oct. 2018.

[14] L. Zhao, D. J. Thrimawithana, U. K. Madawala, A. P. Hu, and C. C. Mi, "A misalignment-tolerant series-hybrid wireless EV charging system with integrated magnetics," *IEEE Trans. Power Electron.*, vol. 34, no. 2, pp. 1276–1285, Feb. 2019.

[15] L. Zhao, S. Ruddell, D. J. Thrimawithana, U. K. Madawala, and P. A. Hu, "A hybrid wireless charging system with DDQ pads for dynamic charging of EVs," in *Proc. IEEE PELS Workshop Emerg. Technol. Wireless Power Transf.*, 2017, pp. 1–6.

[16] M. Budhia, J. T. Boys, G. A. Covic, and C.-Y. Huang, "Development of a single-sided flux magnetic coupler for electric vehicle IPT charging systems," *IEEE Trans. Ind. Electron.*, vol. 60, no. 1, pp. 318–328, Jan. 2013.

[17] U. Madawala and D. Thrimawithana, "Current sourced bi-directional inductive power transfer system," *IET Power Electron.*, vol. 4, no. 4, pp. 471–480, 2011.

[18] G. Kalra, D. J. Thrimawithana, B. S. Riar, C.-Y. Huang, and M. Neuburger, "A novel boost active bridge based inductive power transfer system," *IEEE Trans. Ind. Electron.*, to be published, 2019.

[19] S. Samanta, A. K. Rathore, and D. J. Thrimawithana, "Bidirectional current-fed half-bridge (C)(LC)–(LC) configuration for inductive wireless power transfer system," *IEEE Trans. Ind. Appl.*, vol. 53, no. 4, pp. 4053–4062, Jul./Aug. 2017.

[20] P. Si, A. P. Hu, S. Malpas, and D. Budgett, "A frequency control method for regulating wireless power to implantable devices," *IEEE Trans. Biomed. Circuits Syst.*, vol. 2, no. 1, pp. 22–29, Mar. 2008.

[21] A. P. Hu, J. Boys, and G. Covic, "Frequency analysis and computation of a current-fed resonant converter for ICPT power supplies," in *Proc. Int. Conf. Power Syst. Technol.*, vol. 1, 2000, pp. 327–332.

[22] A. Kamineni, M. J. Neath, G. A. Covic, and J. T. Boys, "A mistuning-tolerant and controllable power supply for roadway wireless power systems," *IEEE Trans. Power Electron.*, vol. 32, no. 9, pp. 6689–6699, Sep. 2017.

[23] D. J. Thrimawithana and U. K. Madawala, "Analysis of split-capacitor push–pull parallel-resonant converter in boost mode," *IEEE Trans. Power Electron.*, vol. 23, no. 1, pp. 359–368, Jan. 2008.

[24] L. Zhao, D. J. Thrimawithana, U. K. Madawala, S. Ruddell, and P. Illenberger, "A push-pull converter based BD-IPT system for wireless grid integration of EVs," in *Proc. IEEE Power Energy Conf. Illinois*, 2016, pp. 1–6.

[25] A. Zaheer, H. Hao, G. A. Covic, and D. Kacprzak, "Investigation of multiple decoupled coil primary pad topologies in lumped IPT systems for interoperable electric vehicle charging," *IEEE Trans. Power Electron.*, vol. 30, no. 4, pp. 1937–1955, Apr. 2015.

[26] Y. G. Su, L. Chen, X. Y. Wu, A. P. Hu, C. S. Tang, and X. Dai, "Load and mutual inductance identification from the primary side of inductive power transfer system with parallel-tuned secondary power pickup," *IEEE Trans. Power Electron.*, vol. 33, no. 11, pp. 9952–9962, Nov. 2018.

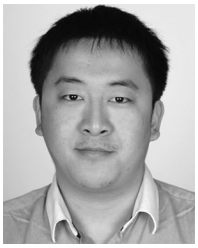

Lei Zhao (S'14–M'19) received the B.Sc. Eng. degree from the Xi'an University of Technology, Xi'an, China, in 2011, and the M.Sc. Eng. degree from the University of Auckland, Auckland, New Zealand, in 2013, both in electrical engineering.

He joined the Department of Electrical, Computer, and Software Engineering, The University of Auckland, in February 2019, where he is currently a Research Fellow with Prof. Aiguo Patrick Hu. His research interests mainly focused on the optimization of the bidirectional hybrid inductive power transfer systems and application of wireless power transfer in consumer electronics.

Duleepa J. Thrimawithana (M'09–SM'18) received the B.E. degree in electrical engineering (with First Class Hons.) and the Ph.D. degree in power electronics from The University of Auckland, Auckland, New Zealand, in 2005 and 2009, respectively.

He joined the Department of Electrical, Computer, and Software Engineering, The University of Auckland, in 2009, where he is currently a Senior Lecturer. He has coauthored more than 100 international journals and conference publications and has filled 18 patents on wireless power transfer technologies. In recognition of his outstanding contributions to engineering as an Early Career Researcher, he received the Jim and Hazel D. Lord Fellowship in 2014. His main research interests include wireless power transfer, power electronics, and renewable energy.

Udaya Kumara Madawala (S'88–M'93–SM'06–F'18) received the B.Sc. degree in electrical engineering (Hons.) from The University of Moratuwa, Moratuwa, Sri Lanka, in 1986, and the Ph.D. degree in power electronics from The University of Auckland, Auckland, New Zealand, in 1993, as a Commonwealth Doctoral Scholar.

He is currently a Full Professor, and focuses on a number of power electronics projects related to wireless (bidirectional) grid integration of electric vehicles for vehicle-to-grid applications and renewable energy. He has more than 300 IEEE & IET journals and conference publications, holds a number of patents related to wireless power transfer and power converters, and is a Consultant to industry.

Dr. Madawala is a Distinguished Lecturer of the IEEE Power Electronic Society, and has more than 30 years of both industry and research experience in the fields of power electronics and energy. He has served both the IEEE Power Electronics and Industrial Electronics Societies in numerous roles, relating to editorial, conference, advisory, technical committee, and chapter activities. He is currently an Associate Editor for IEEE TRANSACTIONS ON POWER ELECTRONICS, and a Member of both the Administrative Committee and Membership Development Committee of the IEEE Power Electronics Society. He was the General Chair of the 2nd IEEE Southern Power Electronics Conference (SPEC) 2016, held in New Zealand, and is also the Chair of SPEC Steering Committee.

Aiguo Patrick Hu (M'01–SM'07) received the B.E. and M.E. degrees from Xian JiaoTong University, Xian, China, in 1985 and 1988, respectively, and the Ph.D. degree from the University of Auckland, Auckland, New Zealand, in 2001.

Funded by Asian 2000 Foundation, he stayed in National University of Singapore as an Exchange Postdoctoral Research Fellow. He is a Leading Researcher in wireless power technologies. He is a Full Professor with the Department of Electrical Computer and Software Engineering, The University of Auckland. He was also the Head of Research of PowerbyProxi Ltd. He has been a Foreign Expert Reviewer of 973 projects for the Chinese Ministry of Science and Technology, and an Assessor of ChangJiang Scholars for Ministry of Education. He holds more than 50 patents in wireless power transfer and microcomputer control technologies, published more than 200 peer-reviewed journals and conference papers with over 4000 citations, authored the first monograph on wireless inductive power transfer technology, and contributed four book chapters on inductive power transfer control as well as electrical machines. His research interests include wireless/contactless power transfer systems and application of power electronics in renewable energy systems.

Dr. Hu is the former Chairman of IEEE NZ Power Systems/Power Electronics Chapter. He was the recipient of the University of Auckland VC's Funded Research and Commercialization Medal in April 2017.